WIMRC 3rd International Cavitation Forum 2011
University of Warwick, UK, 4th-6th July 2011

Cloud Cavitation and Cavitation Erosion in Convergent Divergent Nozzle

T. Keil, P. F. Pelz*, U. Cordes, G. Ludwig
Technische Universität Darmstadt
Chair of Fluid Systems Technology
Magdalenenstraße 4, 64289 Darmstadt
Germany

Peter.Pelz@fst.tu-darmsatdt.de

ABSTRACT

The influence of flow parameters such as cavitation and Reynolds number on the cavitating cloud behaviour and their aggressiveness are analysed in an experimental work.

The geometry under focus is a convergent-divergent nozzle with a given radius of curvature at the minimum cross section. By means of a high-speed camera the kinematics of cloud cavitation is visualized. The aggressiveness of the cloud is quantified by using soft metal layers adapted on the nozzle geometry. The interpretation of the plastic deformation, called pits, is done via a 2-dimensional optical measurement system, which is developed to scan large and curved surfaces. By doing this damage maps are gained.

Consequently dimensional analysis is used, to analyse and generalize the experimental findings. Thus a critical Reynolds number is found for the transition from sheet to cloud cavitation. Further an upper limit for the Strouhal number is found for the given geometry.

NOMENCLATURE

letter

E	plastic deformation energy	ML^2T^{-2}
f	frequency	T^{-1}
H	channel height	L
h	nozzle height	L
L	sheet length	L
L_m, l_m	material length	L
p	pressure	$ML^{-1}T^{-2}$
Q	volume flow	L^3T^{-1}
R	radius	L
Re	Reynolds number	-
St	Strouhal number	-
U	velocity	LT^{-1}
x	coordinate	L
Γ	circulation	L^2T^{-1}
σ	cavitation number	-
ρ	density	ML^{-3}
λ	non-dim. sheet length	-
γ	non-dim. Circulation	-
π	non-dim. damage energy	-
ϑ	yield stress	$ML^{-1}T^{-2}$
κ	geometry parameter	-
ν	kinematic viscosity	L^2T^{-1}

indices

E	inlet
A	outlet
V	vapor
+	dimension less

1. INTRODUCTION

One of the more aggressive cavitation forms is cloud cavitation which is observed above a critical Reynolds number as will be shown within this paper. The high aggressiveness of cloud cavitation was reported by several researchers (e. q.

[1], [2] and [3]). It is now understood that the cloud plays a key role in **the temporal and special energy focusing cascade** which is essential for the cavitation erosion process. The stationary energy flux of the incoming flow is concentrated in time and space in the form of clouds. As a single bubble the cavitation cloud becomes unstable when it reaches a critical size. The critical size depends on the growth rate, the initial size and the initial vapor content of the cloud [15]. When the cloud collapses the second energy focusing process starts: Like a single bubble when collapsing the cloud imposes a sink flow and focuses the kinetic energy of the surrounding fluid in its center.

The intensity of the collapse and thus the aggressiveness is determined by the dynamic behavior and by the type of the occurring structures.

Konno and Kato [3] employed a numerical model to describe the dynamic behavior of a cloud cavitation floating off from a hydrofoil. Similar investigations on a cavitating nozzle flow have been conducted by Wang [5].

The results of our experimental work presented in this paper the cloud kinematics is analyzed by using a high-speed camera. In addition, the aggressiveness of cavitation erosion is assessed by using soft metal layers, used as a material sensor. This approach offers the possibility to evaluate damage distributions and damage intensities. To quantify the effective damage energy a developed so-called pit-count measurement system is used, which detects the size and the position of each pit on the

damaged surface. The effective damage energy and thereby the cavitation aggressiveness is evaluated by a here introduced dimensionless damage function.

2. EXPERIMENTAL SET UP AND PARAMETER

The necessary requirements for the test rig are (i) an excellent optical accessibility, (ii) the possibility to vary the geometries curvature, and (iii) to provide an installation-opportunity for soft metal layers which serve as material sensors.

The optical access (i) is realized by a channel having rectangular cross section and walls completely made of acrylic glass. The high-speed observations are illuminated with a stroboscope for the top view perspective, for the side view perspective a laser light sheet is used. The adaptation of the copper layer (iii) is implemented directly behind the narrowest cross-section area. To initiate evenly the cavitation over the whole nozzle width, a wire with rectangular cross section seen in Fig. 1 is placed in the smallest cross section area. By doing this every side wall friction influences due to surface roughness are small in comparison to the wire influence and such not visible in the experiments.

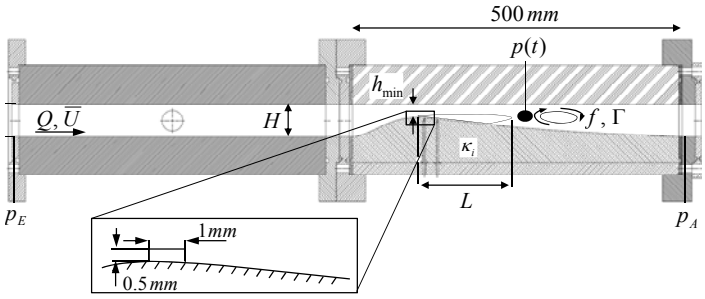

Fig. 1: Nozzle test rig at the Chair of Fluid Systems Technology.

The nozzle shape is given by the dimensionless function

$$h_+(x_+) = \frac{\text{const.}}{\exp\left(\frac{x_+}{\kappa_1}\right) + \exp\left(\frac{x_+}{\kappa_2}\right)}, \tag{1}$$

where the height h and the axial length x are made dimensionless by the channel height H. Within this paper we present and discuss only one radius of curvature $R_+ = 2.5$ determined by the two free parameters κ_1 and κ_2. The influence of both free parameters on the radius of curvature in the smallest cross section is shown in Fig. 2. The filled circle indicates the geometry being under research.

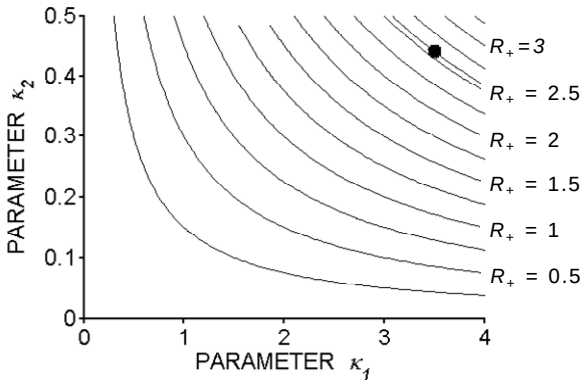

Fig. 2: Radius of curvature for the shape function (1).

The cavitation behavior is influenced by variation of the cavitation number and the Reynolds number, respectively the outlet pressure p_A and the cross section averaged flow velocity $\bar{U}$ (see Fig. 1):

$$\sigma = \frac{p_A - p_V}{\frac{\rho}{2}\bar{U}^2}, \tag{2}$$

$$\mathrm{Re} = \frac{\bar{U}H}{\nu}, \tag{3}$$

where ν is the kinematic viscosity, ρ the density and p_V the vapor pressure of water.

For cloud cavitation the most relevant physical parameters are the shedding frequency f of the cavitation cloud, the typical size L of the sheet and the circulation Γ of the cloud. The associated dimensionless relations

$$\frac{fH}{\bar{U}} = \mathrm{St}(\mathrm{Re}, \sigma, \kappa_i), \tag{4}$$

$$\frac{L}{H} = \lambda(\mathrm{Re}, \sigma, \kappa_i), \tag{5}$$

$$\frac{\Gamma}{\bar{U}H} = \gamma(\mathrm{Re}, \sigma, \kappa_i), \tag{6}$$

are measured.

With (4), (5), (6) the largest scales of the periodic cavitation process are given. In fact cloud cavitation is similar to vortex shedding in the wake of a body. Only the physical mechanism is different. The vorticity and hence the circulation have their origin in the baroclinic source term of the vorticity equation where for vortex shedding the vorticity has its origin in the diffusion term on the right hand side of the vorticity equation.

3. EXPERIMENTAL RESULTS

High-Speed Observation

The high-speed images from the top view (Fig. 3) show a cavitation cloud formed from a cavitation sheet. The process is evaluated by a software tool detecting the front edge of the sheet and of the cloud.

The periodic process starts by the growth of the cavitation sheet to its maximum sheet length L. While the sheet grows, the so-called 're-entrant jet' flows underneath the cavitation sheet from its trailing to its leading edge. The up breaking cavitation volume forms a cavitation cloud showing a circulation which is determined by the developing process. After the cloud has separated the process starts again.

During the growth process, the furled cloud is observed in Fig. 3 a), b) and c) marked with the white lines. The cloud remains in the wake of the growing sheet cavitation, which can be seen by the stagnation of the rolled-up cloud. During this time period, the cloud is embossed a circulation.

The lower pressure in the vortex core leads to a decreasing of the static pressure, which is measured by a fast scanning pressure sensor installed at the channel wall 65 mm downstream of the smallest cross section area. On the other site the cloud collapse produces a pressure peak, which is also recorded and qualitatively shown in Fig. 3 f).

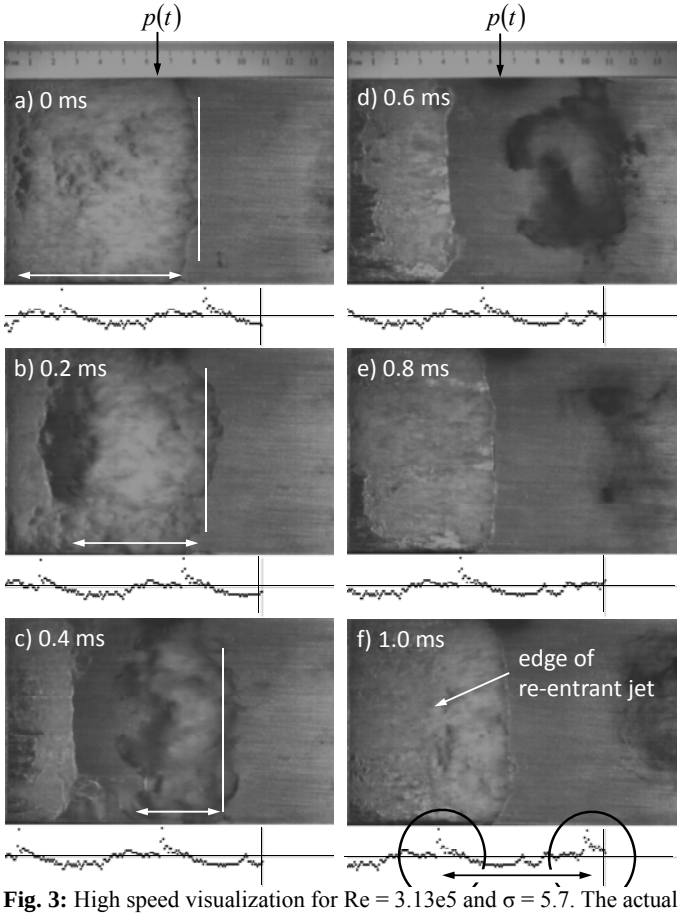

Fig. 3: High speed visualization for Re = 3.13e5 and σ = 5.7. The actual pressure signal is shown in the diagram below the pictures.

The periodic behavior of the flow is visible from the pressure timeline shown in Fig. 3.

The Fourier transform of both time histories, i.e. position of the front and pressure, are shown in Fig. 4.

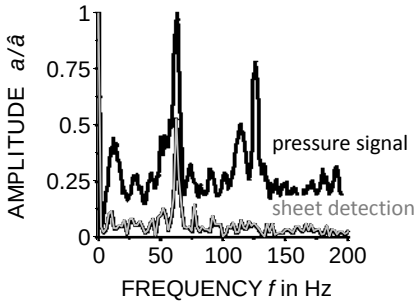

Fig. 4: -Fourier transform of the pressure history and the position of the sheet front.

The analysis of both signals show a clear typical frequency associated with the cloud shedding.

Strouhal Number vs. Reynolds and Cavitation Number

Fig. 5 shows the Strouhal number (4) as a function of cavitation and Reynolds number.

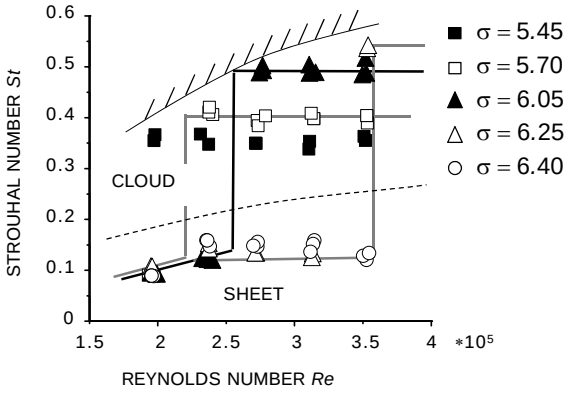

Fig. 5: Transition from sheet to cloud cavitation.

There are two characteristic flow regimes (shown in Fig. 5 and Fig. 6). For a given cavitation number there is a critical Reynolds number. (i) for Reynolds number smaller that critical value we observe sheet cavitation without cloud shedding. (ii) above that critical Reynolds number we observe cloud cavitation. The Strouhal number is in that case independent of the Reynolds number. Hence there should be no dependence on the size of the device in that flow regime.

A critical velocity was first described by Arndt [6]. Here we have the velocity made dimensionless by the kinematic viscosity and the channel height (i.e. Reynolds number).

For the highest cavitation number of 6.4 we could not observe a critical Reynolds number. (But there might be such a number outside the operation range of our test rig.)

By reducing the cavitation number at a given Reynolds number the sheet length increases until again a stability limit is reached. The transition is associated with a sudden increase of the Strouhal number to its maximum value at a given Reynolds number. The limiting curve is roughly indicated in Fig. 5 by the most upper line. A further reduction of the cavitation number leads to an enlargement of the sheet length and thus to a reduction in the Strouhal number. The decrease of the cavitation number finally leads to full cavitation (flashing) just above the dotted line in Fig. 5. The Fig. 6 shows the dependence of the Strouhal number on the cavitation number.

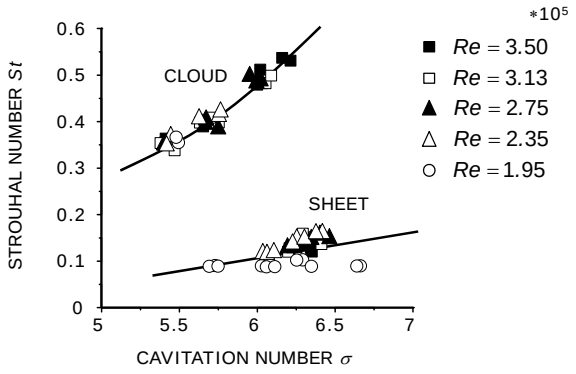

Fig. 6: Strouhal number vs. cavitation number.

Of course all the findings depend on the shape of the nozzle. Presumably on mayor parameter is the minimal radius of surface curvature, which is the main parameter to be changed for our future research.

Sheet Length and Circulation of the Cloud

Fig. 7 shows the maximum sheet length L and Fig. 8 typical velocities characterized by the sheet cavitation as a function of the cavitation number. The Reynolds number has for cloud cavitation no influence as again Fig. 7 and Fig. 8 indicate.

These general results justify model test of pumps or turbines with respect to cloud cavitation!

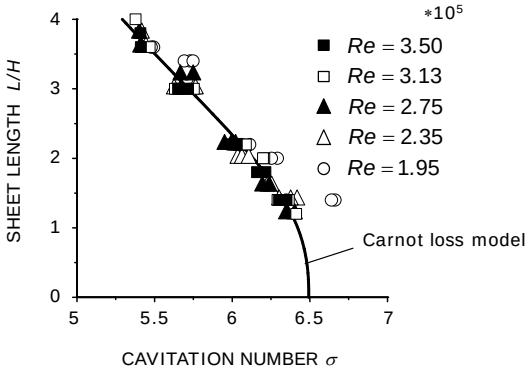

Fig. 7: Sheet length vs. cavitation number. The Reynolds number has no influence on the sheet length. The solid line indicates a Carnot loss model.

The growing size of the cavitation sheet for a decrease of the cavitation number causes a throttling of the flow. A simple fluid mechanical model based on Carnot's shock loss is sufficiently accurate to predict the experimental results (solid line in Fig. 7).

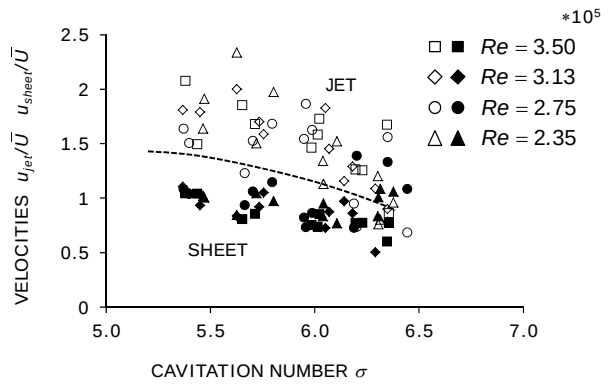

Fig. 8: Mean velocity of the growing sheet cavitation and the velocity of the re-entrant jet.

Fig. 8 shows the mean velocities of the sheet growth $u_{sheet}/\bar{U}$ and of the re-entrant jet $u_{jet}/\bar{U}$.

The sheet and jet velocities are determined by means of the optical measurements and are time averaged velocities. As Fig. 8 shows, the velocities do not depend on the Reynolds number.

A second point to mention is the difference in the velocities. The difference cannot be explained by classical free-streamline theory. A third point to mention is the mean sheet velocity, being close to the velocity of the incoming flow. The mean flow velocity at the minimal cross section is by a factor of 2.5 higher than the sheet velocity. Again this difference is surprisingly large from a classical fluid mechanics point of view: We expected a sheet velocity of roughly 2.5.

To quantify the circulation, the closed integral over the sheet is evaluated by using the mean values of the determined velocities u_{sheet} and u_{jet}.

$$\gamma = \frac{\Gamma}{\bar{U}H} = \frac{L}{H}\frac{u_{sheet}+u_{jet}}{\bar{U}}. \qquad (7)$$

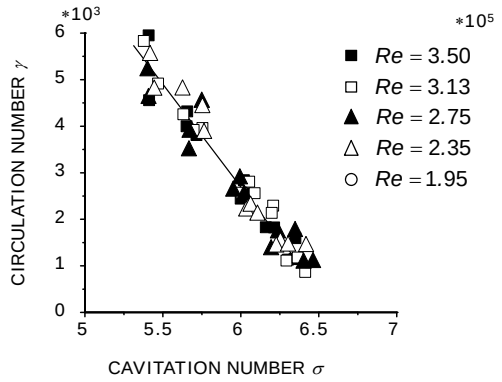

Fig. 9: Dimensionless circulation number vs. cavitation number.

An increased cavitation length, i.e. decreased cavitation number, results in an increased circulation numbers as shown in Fig. 9.

To summarize the results gained so far: As soon a critical Reynolds number is reached, there is a periodic cloud shedding and the Reynolds number vanishes on the right hand side of (4), (5), (6): $f\bar{U}/H = St(\sigma, \kappa_i)$, $L/H = \lambda(\sigma, \kappa_i)$, $\Gamma/\bar{U}H = \gamma(\sigma, \kappa_i)$.

It is important to mention:

Our results justify the model test for pumps and turbines. Only the Reynolds number has to be for the model above the critical Reynolds number.

4. PLASTIC DEFORMATION OF SOLID SURFACE DUE TO CLOUD CAVITATION

Automated Pit-Count System

Pit-count is a measurement principle to detect plastic deformations on polished metal surfaces developed at the Chair of Fluid Systems Technology by Lohrberg [9]. Curved surfaces are scanned by an all-in-focus algorithm. The surface is scanned before and after a cavitation experiment. By comparing the two scans, a filter algorithm is implemented to distinct between materials defects from pits, which are the result instable cavitation bubbles. Such a pit is shown in Fig. 10.

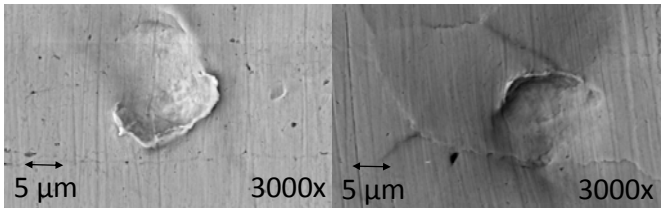

Fig. 10: Plastic deformations of a copper surface after 30 min and dislocation movements of gains after 300 min, σ = 0.112

The pit-count software gives finally a damage map of the curved surface.

The creation of damage maps with a local damage distribution with known radius and position of all plastic deformation are possible. The damage energy can be calculated by using an empirical relationship developed and used by Lohrberg [9].

$$E = \vartheta L_m^3 \sum \left(1 + \frac{R_i}{l_m}\right)^3, \qquad (8)$$

where ϑ is the yield stress of the material, L_m and l_m are two material typical lengths. R_i is the pit radius.

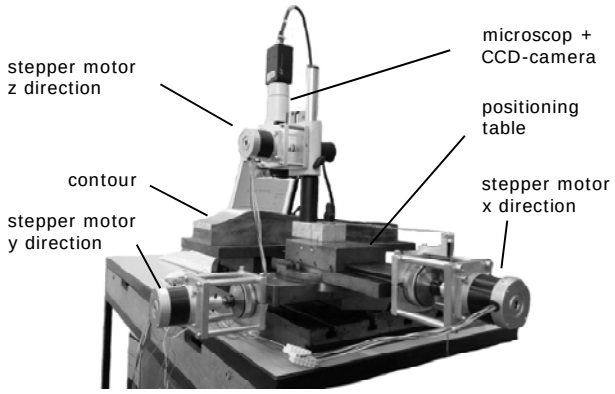

Fig. 11: Fully automated pit-count system at the Chair of Fluid Systems Technology.

Damage Maps

Pit count measurements are carried out for Reynolds numbers 2.75e5 and 3.5e5 and the cavitation numbers 5.45, 5.7, 6.05. Fig. 5 shows those operation points to lay complete within the cloud regime.

Fig. 12 shows the damage maps for a Reynolds number of 2.75e5 and the three named cavitation numbers 5.45, 5.7, 6.05 The exposure time $T = 90\text{min}$ is made dimensionless by the shedding frequency. Thus fT gives the load cycles on the surface. The number of load cycles is given for each experiment in Fig. 12 (and Fig. 13).

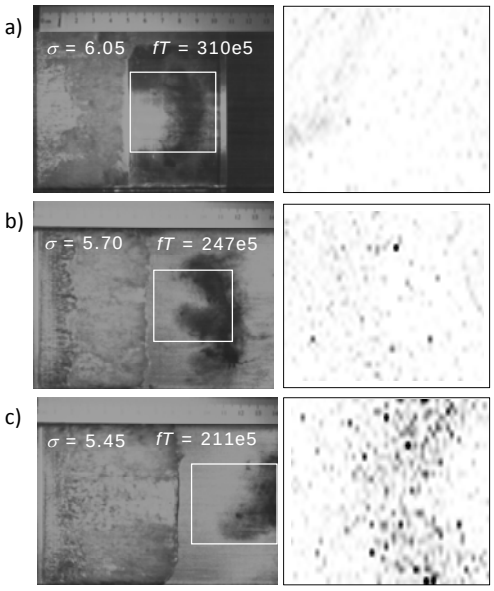

Fig. 12: Damage maps for the cavitation numbers 5.45, 5.7, 6.05 at a small Reynolds number of 2.75e5.

As expected, a smaller cavitation number results in an increased cavitation zone and thus an increased damage during exposure time.

Fig. 13 shows the experimental results for the larger Reynolds number of 3.5e5. The load cycles are again given within the pictures.

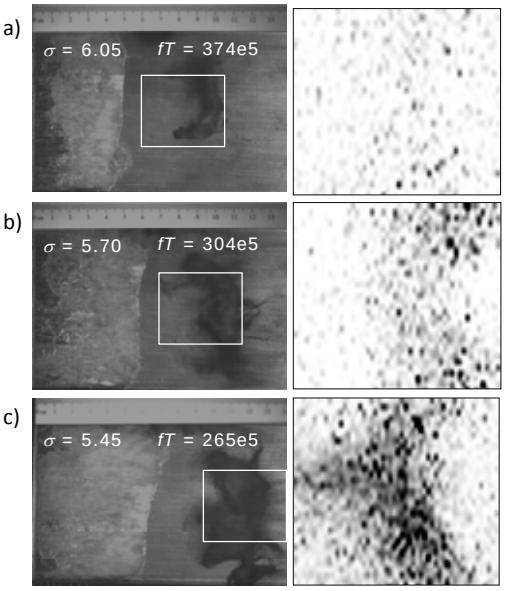

Fig. 13: Damage maps for the cavitation numbers 5.45, 5.7, 6.05 at a small Reynolds number of 3.5e5.

To compare the experimental results the deformation energy is accumulated for the whole polished surface using the empirical relation (8) is calculated.

To make different flow conditions comparable, it has shown to be use full to normalize the deformation energy (9) as:

$$\frac{E}{\rho \bar{U}^2 H^3 fT} = \pi(\mathrm{Re}, \sigma, \kappa_i). \tag{9}$$

In order to compare the aggressiveness of operating points, the non-dimension energy is based on the number of damage cycles fT in Eq. (9). The result is shown in Fig. 14, were the accumulated dimensionless damage energy per cycle is given as a function of the cavitation number.

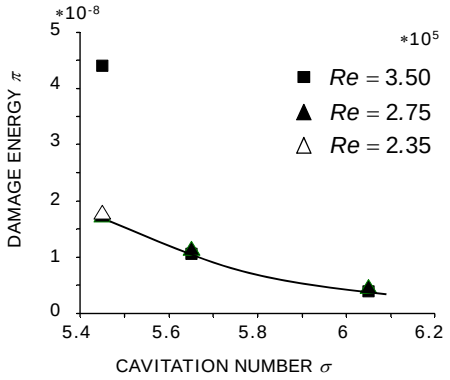

Fig. 14: Dimensionless damage energy per damage cycle.

Up to the point Re=3.5e5 at the lowest cavitation number (see damage map shown in Fig. 13. c)), all results are on one line. To show the influence of the Reynolds number for small cavitation numbers an operating point for a Reynolds number at 2.35e5 is added in the measurement program.

Fig. 15 shows the first moment of the damage maps given in Fig. 12 and 13 normalized with the channel height.

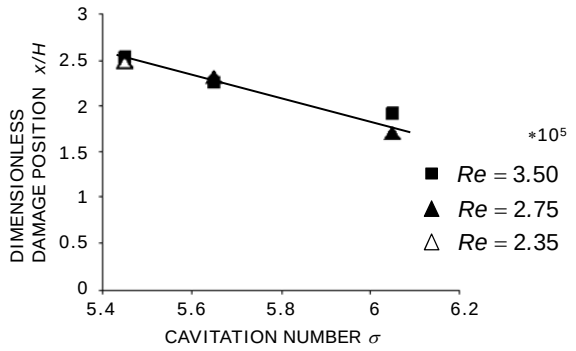

Fig. 15: Dimensionless damage position is independent of the Reynolds number but depends on cavitation number.

The damage position is primarily influenced by the cavitation number and thus by the sheet length.

5. CONCLUSIONS

For a convergent divergent nozzle, a critical Reynolds number is determined. For Reynolds numbers below that critical value sheet cavitation is observed. For Reynolds number above that critical value cloud cavitation is observed. The nozzle geometry is such, that the minimal radius of curvature can easily be changed. Up to now the radius of curvature was set to 2.5 times the channel height.

By optical measurements the largest scales of the cavitation phenomena were determined.

An upper limit for the Strouhal number was observed. That upper limit is dependent on the Reynolds number.

For the first time the circulation of clouds was determined.

Within the cloud regime there is no influence on the Reynolds number, which justifies model test of pumps and turbines.

A dimensionless damage function was defined and the plastic deformation of the material surface was determined as a function of cavitation number.

ACKNOWLEDGMENTS

The presented results were obtained within the research project No. 16054 N/1, funded by budget resources of the Bundesministerium für Wirtschaft und Technologie (BMWi) approved by the Arbeitsgemeinschaft industrieller Forschungsvereinigungen “Otto von Guericke” e.V. (AiF).

REFERENCES

[1] Ida, M., *Investigation of transition frequencies of two acoustically coupled bubbles using a direct numerical simulation technique*, J. Phys. Soc. Jpn., 2004

[2] Ida, M., *Multibubble cavitation inception*, J. Phys. Soc. Jpn., 2009

[3] Konno, A., Kato, H., Yamaguchi, H., Maeda, M., *On the collapsing behavior of cavitation bubble clusters*, JSME International Journal, Series B, Vol. 45, No. 3, 2002

[4] Kubota, A., Kato, H., Yamaguchi,H., *A new modelling of caviting flows: a numerical study of unsteady cavitation on a hydrofoil section*, J. Fluid Mech. (1992), vol. 240, pp 59-96, 1992

[5] Wang, Y.-C., *Shock Waves in bubbly cavitating flows; (Part I.) Shock Waves in Cloud Cavitation; (Part II.) Bubbly cavitating flows Through a converging-diverging nozzle*, California Institute of Technology Pasadena, California, 1996

[6] Arndt, R.E.A., Hambleton, W.T., Kawakami, E., *Creation and maintenance of cavities under horizontal surfaces in steady and gust flows*, Journal of Fluid Engineering, Nov. 2009, Vol 131 /111301-1, 2009

[7] Kawanami, Y., Kato, H., Yamaguchi, H., Maeda, M., Nakasumi, S., *Inner Structure of Cloud Cavity on a Foil Section*, JSME International Journal, Series B, Vol. 45, No 3, 2002

[8] Joussellin, F., Delannoy, Y., Sauvage-Boutar, E., Goirand, B., *Experimental Investigations on Unsteady Attached Cavities*, Proc. ASME FED, Vol. 116 (1991), pp. 61-66

[9] Lohrberg, H., *Messung und aktive Kontrolle der erosiven Aggressivität der Kavitation in Turbomaschinen*, Fortschritts-Bericht VDI Reihe 8 Nr. 942 ISBN 3-18-394208-5, 2001

[10] Schmid, P.J., *Dynamic mode decomposition of numerical and experimental data*, J. Fluid Mech. (2010), vol. 656, pp. 5-28, 2010

[11] Schmid,P.J., Li, L., Juniper, Pust, O., *Applications of the dynamic mode decomposition*, Theor. Comput. Fluid Dyn., DOI 10.1007/s00162-010-0203-9, 2009

[12] Van Terwisga, Fitzsimmons, P.A., Ziru, L., Foeth, E.J., *Cavitation Erosion – A review of physical mechanisms and erosion risk models*, Proc CAV2009 – 7th International Symposium on Cavitation, Ann Arbor, 2009

[13] Fortes Patella, R., Reboud, J.L., *Interaction between pressure waves and spherical cavitation bubbles: Discussion about cavitation erosion mechanism*, Proc. Of the 2000 ASME Fluids Engineering Summer Conference, Boston, Massachusetts, 2000

[14] Fortes Patella, R., Challier, G., Reboud, J.L., Archer, A., *Cavitation erosion mechanism: numerical simulations of the interaction between pressure waves and solid boundaries*, Proc. CAV2001 International Symposium on Cavitation, Pasadena, 2001

[15] Pelz, P., Keil, T., Buttenbender, J., *On the transient behavior of cloud cavitation*, SHF conference on Cavitation and Hydraulic Machines, Lausanne workshop, May 26-27 2011